Multiple layers of self-asssembled Ge/Si islands: Photoluminescence, strain fields, material interdiffusion, and island formation

O. G. Schmidt and K. Eberl
Max-Planck-Institut für Festkörperforschung, Heisenbergstraße 1, 70569 Stuttgart, Germany
(Received 4 June 1999; revised manuscript received 27 August 1999)

Strain fields in stacked layers of vertically aligned self-assembled Ge islands on Si(100) can cause a reduction of the wetting layer thickness in all but the initial layer and hence induce an energy separation ΔE_{wl} between the energy transitions of the different wetting layers. Our systematic photoluminescence (PL) study on twofold stacked Ge/Si layers shows that the quantity ΔE_{wl} is a sensitive function of the Si spacer thickness and reflects the degree of strain field interaction between the island layers. Pronounced PL blueshifts are also observed for the island related energy transition in twofold and multifold island layers. We suggest that with increasing number of stacked island layers strain field superposition of buried islands causes enhanced SiGe material intermixing during Si overgrowth of the islands. This effect naturally explains the strong PL blueshift of the island related energy transition. Recently observed shape transformations in stacked Ge islands are well explained by our model of superimposed strain fields. We also discuss the initial stages of island formation in the second Ge layer of twofold island stacks. Many of the effects observed in this paper on the Ge/Si system are probably also important for self-assembling III/V islands but due to extremely small sizes are much harder to evaluate.

I. INTRODUCTION

An approach to reduce the inhomogeneity of self-assembled Ge dot structures is the fabrication of multilayer island stacks. In this geometry strain fields of underlying islands penetrate into the spacer layer, create a strain energy modulation at the surface, and induce stacks of vertically aligned[1–4] and laterally more homogeneous islands in upper layers.[5,6]

Among the many different material systems the lattice mismatched Si/Ge system is particularly well suited for fundamental studies on structural, electronic, and optical properties of self-assembled islands since growth conditions can be chosen in such a way that both the island related and the wetting layer (WL) related energy transitions are equally well-resolved in photoluminescence (PL) experiments.[7,8]

Only very recently, it was found that the strain field modulation induced by an initial Ge island layer causes a reduction of the wetting layer thickness t_{wl} in upper layers[9] and induces an energy separation ΔE_{wl} of the WL related energy transition. However, the system investigated was rather complex and needed further investigations to understand the effects of strain fields in Ge/Si multiple island layers.

This paper presents a systematic PL study of two and multiple Ge/Si island stacks with special attention given to the effects of generated strain fields. The paper is organized as follows: In Sec. II we describe the growth procedure and measurement details. In Sec. III we focus on two pairs of Ge/Si layers where we systematically vary the Si spacer layer thickness t_s and investigate the strain field penetration between the layers. We find that ΔE_{wl} depends sensitively on the strain field interaction between the two island layers and we show that ΔE_{wl} can probe the strain fields originating from a buried island layer. In Sec. IV we present PL data of multiple Ge/Si island layers where the effects for twofold island stacks are successively repeated with each added Ge/Si bilayer. Based on our experimental data we evaluate the tensile strain component at the Si growth front after each capped island layer and compare our calculations to ΔE_{wl} for multiple Ge/Si layers. In Sec. V we discuss the implications of our model for SiGe intermixing during Si overgrowth of Ge islands and suggest that it is indeed the effect of SiGe alloying that causes the pronounced PL blueshift for the islands. Recently observed shape transformations in buried islands are also explained by our model. Finally we focus in Sec. VI on the initial stage of island formation in the second layer of twofold island stacks.

II. EXPERIMENTAL DETAILS

All samples investigated in this work are grown by solid source molecular-beam epitaxy on n^--type Si (001) substrates. After SiO_2 desorption from the Si substrate in the growth chamber at 900 °C, the substrate temperature is ramped down to 400 °C and an about 400 nm-thick Si buffer layer is grown while first ramping the substrate temperature T_g up to 770 °C and then lowering T_s down to the actual growth temperature of the active layers. The active region consists of nominally pure Ge layers separated by Si spacer layers of thicknesses t_s. Since the opening and closing times of the Si and Ge shutters are very different, we introduced a growth interruption of nominal 5 s before and after each Ge layer, which ensures well-defined onsets of epitaxial growth. The samples are capped by a 160 nm-thick Si layer. For some samples identical active layers are grown on the surface for structural analysis. Typical growth rates are 1.3 and 0.07 Å/s for Si and Ge evaporation, respectively. During growth the chamber pressure is about $2-3\times10^{-9}$ mbar starting at a base pressure of about 10^{-11} mbar. The substrate temperature is calibrated by measuring the voltage over a

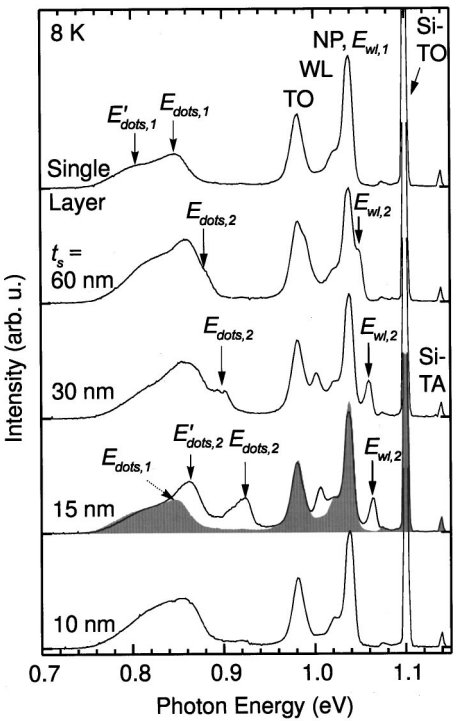

FIG. 1. Photoluminescence spectra of a series of samples where the Si spacer thickness t_s was systematically varied. The top spectrum is taken from a reference sample incorporating only one Ge layer. For all samples the Ge coverage is 5 ML and the growth temperature was 700 °C. The NP lines originating from the first and second wetting layer are indicated by $E_{\mathrm{wl},1}$ and $E_{\mathrm{wl},2}$ $E_{\mathrm{dots},1}$, $E'_{\mathrm{dots},1}$ and $E_{\mathrm{dots},2}E'_{\mathrm{dots},2}$ denote the island related PL peaks in the first and second layer, respectively. The single layer PL spectrum is again inserted as a gray shaded graph for $t_s = 15$ nm.

tungsten thermocouple mounted on an n^--type Si wafer under identical growth conditions.

Structural properties are determined by atomic force microscopy (AFM). PL is excited using the 488-nm line of an Ar^+ laser. The samples are cooled in a He-flow cryostat to a temperature of 8 K. PL is analyzed by a 1-m spectrometer and is detected by a liquid-nitrogen-cooled Ge detector using standard lock-in technique.

III. TWOFOLD ISLAND STACKS

The photoluminescence spectra of a series of samples with twofold stacks of islands, where we systematically varied t_s, is presented in Fig. 1. All samples incorporate 5 ML Ge and were grown at a temperature T_g of 700 °C. The top spectrum is taken from an identical reference sample consisting of only a single Ge layer. Apart from the usual Si-TO and Si-TA lines originating from the Si substrate and epilayers, well-resolved no-phonon (NP) and TO phonon replica are detected from the WL at 1.039 and 0.983 eV, respectively. In the following we will denote the NP line of the initial WL with $E_{\mathrm{wl},1}$. A broader peak at around 0.82 eV originates from the Ge islands and consists of two broad convoluted peaks labeled $E_{\mathrm{dots},1}$ and $E'_{\mathrm{dots},1}$. Similar spectra have been observed in Refs. 4 and 10, where the two peaks have been attributed to the NP and TO phonon energy transition of charge carriers recombining in or at the edge of the islands. We also want to point out an alternative explanation for the existence of the two peaks. These two peaks might originate from a bimodal island distribution that we observe for the selected growth conditions and consists of pyramid shaped islands and multifaceted domes, as has been reported in the literature.[8,11–13] From AFM experiments we deduce a pyramid density of $7.5\times10^8\,\mathrm{cm}^{-2}$ and a dome density of $5.5\times10^8\,\mathrm{cm}^{-2}$. The structural aspects and consequences for PL spectra will be discussed in more detail in Sec. VI.

In the case of stacked layers the spectra undergo a gradual change for $t_s \geqslant 15$ nm. Let us first concentrate on the WL. The WL related PL lines from the single Ge layer are exactly reproduced for the twofold stacks, proving that the lines at lower energy originate from the initial WL and the shifted pair of lines originate from the second WL. The blueshifted NP line of the second WL is denoted with $E_{\mathrm{wl},2}$. We suggest the following physical driving force for this behavior: After the first Ge island layer is capped with Si, a strain field modulation can be found at the Si surface, i.e., there is tensile strain exactly above a buried island and compressive strain at the Si surface between buried islands.[15] This leads to directional migration of deposited Ge atoms into areas with extended Si lattice constants (tensile strain), which causes the vertical island alignment. Additionally, we expect the tendency of atom migration to be a function of the magnitude of the strain field modulation. This means that islands nucleate earlier for stronger strain field modulations and thus cause thinner critical thicknesses and hence thinner wetting layers for thinner Si spacer layers.[9]

A gradual modification of the island related PL peaks with thinner t_s is also apparent. In addition to the peaks $E_{\mathrm{dots},1}$ and $E'_{\mathrm{dots},1}$, a shoulder appears on the high-energy side, which blueshifts with decreasing t_s. We denote this peak with $E_{\mathrm{dots},2}$. For $t_s = 15$ nm the peak $E_{\mathrm{dots},1}$ is convoluted by a second peak $E'_{\mathrm{dots},2}$ at 0.86 eV with comparable line shape as $E_{\mathrm{dots},2}$. For clarity we inserted the single layer spectrum as a light gray shadow onto the spectrum of the twofold island stack. Due to the broad linewidths it is not possible to deconvolute $E'_{\mathrm{dots},2}$ from $E_{\mathrm{dots},1}$ and $E'_{\mathrm{dots},1}$ for $t_s = 60$ and 30 nm. Hence, the two peaks are labeled in Fig. 1 for $t_s = 15$ nm, only.

For $t_s = 10$ nm, $E_{\mathrm{wl},2}$ and $E_{\mathrm{dots},2}$ disappear and only the energetically lower-lying peaks remain. We appoint this effect to charge carrier transfer in neighboring layers where the carriers tunnel into the structure with the deeper localization potential. As a result the PL spectrum of the $t_s = 10$ nm sample looks very similar to the single layer reference sample.

The energy separation of the WL transitions is defined as the difference of the NP energies originating from the first and second WL layers, i.e.,

$$\Delta E_{\mathrm{wl},21} = E_{\mathrm{wl},2} - E_{\mathrm{wl},1}. \tag{1}$$

A summary of $\Delta E_{\mathrm{wl},21}$ as a function of t_s is given in Fig. 2(a). We first concentrate on the series of samples that were grown at 700 °C. The experimental data points lie on a smooth curve, approaching a saturation value of about 26 meV for small t_s and gradually approaching zero for large t_s. For $t_s < 12.5$ nm, $E_{\mathrm{wl},2}$ has disappeared due to charge car-

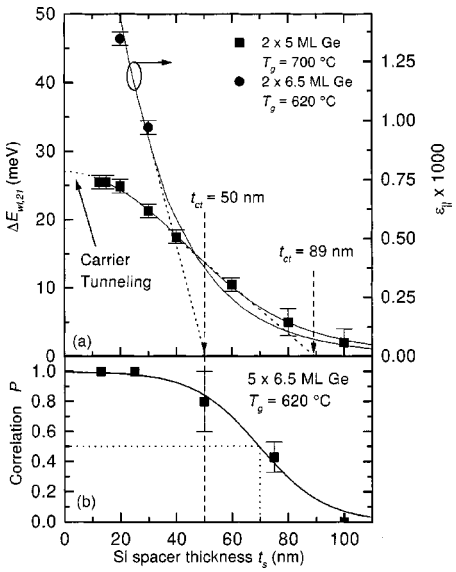

FIG. 2. (a) Wetting layer related line splitting $\Delta E_{\mathrm{wl},21}$ as a function of Si spacer thickness t_s for twofold stacks of islands. Squares and circles represent samples grown at 700 °C and 620 °C, respectively. The in-plane strain $\epsilon_{\|}$ is shown on the right vertical axis, which fits the data of the 620 °C samples well. Extrapolation of the linear regime yields a correlation thickness of $t_{ct}=89$ and 50 nm for the different growth conditions. For $t_s<12.5$ nm ($T_g=700$ °C) the line splitting is not observed due to charge carrier tunneling and the curve is represented by a dotted line in this regime. (b) Vertical correlation probability P as determined by quantitative TEM analysis. We have already published data in (b) in Ref. 1.

rier tunneling in neighboring layers and we represent this part of the curve with a dotted line. $\Delta E_{\mathrm{wl},21}$ can be fitted by a function of the form

$$\Delta E_{\mathrm{wl},21}(t_s)=\frac{A}{1+B(t_s^2)^{3/2}}, \tag{2}$$

where the fitting parameters are taken as $A=26.1$ meV and $B=7.7\times10^{-6}$. The constant A gives the energy separation for $t_s=0$ and the parameter B describes the attenuation behavior of the curve, i.e., the smaller B the longer the strain field penetration into the Si spacer layer. We use Eq. (2) in the next section to determine the strain field superposition in multiple Ge/Si island stacks.

From a qualitative point of view $\Delta E_{\mathrm{wl},21}(t_s)$ seems to directly probe the strain field magnitude above the buried islands, i.e., for small t_s the strain fields directly above the initial islands are still strong and cause a large reduction in t_{wl} and hence larger confinement energies, whereas for large t_s the strain field modulation at the growth front has decreased and t_{wl} approaches its value for a single island layer. To make this point very clear we want to stress that the energy separation $\Delta E_{\mathrm{wl},21}(t_s)$ is *not* caused by different band offsets modified by the strain fields of the buried islands, but is due to the larger confinement energies in a thinner wetting layer due to the earlier island nucleation in the second layer, which is initiated by the penetrating strain fields of the buried islands.

In the following we show that the existence of the energy separation $\Delta E_{\mathrm{wl},21}$ is not exclusive to the specific growth condition chosen above but is also observable for very different growth temperatures and Ge depositions. We also check to what extent $\Delta E_{\mathrm{wl},21}$ can be used to evaluate the strain field above a buried island. For this purpose we insert $\Delta E_{\mathrm{wl},21}(t_s)$ for two samples with 6.5-ML Ge, which are grown at $T_g=620$ °C. As expected we record a pronounced energy separation for this growth temperature, too. Obviously, different growth conditions can change $\Delta E_{\mathrm{wl},21}$ substantially. For example, at a fixed Si spacer layer thickness $t_s=20$ nm, the energy separation $\Delta E_{\mathrm{wl},21}$ is 47 meV for the sample grown at 620 °C and only 25 meV for the sample grown at 700 °C. We also depict the in-plane strain component $\epsilon_{\|}$ above a buried island along the growth direction z in Fig. 2(a). $\epsilon_{\|}$ was determined from finite element calculations using a method similar to that described in Refs. 9 and 14. The geometry of the islands was assumed similar to that seen in cross-section TEM images taken from islands grown under the same conditions.[9] We see that the two experimental points are well described by $\epsilon_{\|}$ except that the slope of $\epsilon_{\|}$ is slightly larger than for the measured data points. In the following heuristic model we assume that the energy separation $\Delta E_{\mathrm{wl},21}$ is proportional to $\epsilon_{\|}(z)$:

$$\Delta E_{\mathrm{wl},21}(t_s)=C\epsilon_{\|}(z), \tag{3}$$

where C is a constant if identical growth conditions are applied for each t_s. We expect C to change if growth conditions change, as we have observed in Fig. 2(a). The connection between strain and $\Delta E_{\mathrm{wl},21}$ in Eq. (3) is very useful since it opens easy experimental access to the strain-field behavior above buried islands.

The changeover from strict vertical island alignment to random island distribution in stacked island layers is not abrupt but is gradual.[1,2,15] It would be practical to have a well-defined and characteristic quantity, viz, a correlation thickness t_{ct}, which evaluates this transition regime. A simple method to define such a quantity is the intersection of the tangent at the turning point of $\Delta E_{\mathrm{wl},21}(t_s)$ with $\Delta E_{\mathrm{wl},21}=0$. In Fig. 2 this method yields a correlation thickness t_{ct} of 89 nm for $T_g=700$ °C and 50 nm for $T_g=620$ °C. The difference in t_{ct} nicely illustrates that although absolute values of $\Delta E_{\mathrm{wl},21}$ can be larger for low T_g, the actual interaction distances of the underlying strain fields can be considerably smaller. This result is easy to understand: On the one hand, at lower growth temperatures, island dimensions tend to be smaller[4,8,16] creating strain fields of shorter range. On the other hand, material intermixing is less pronounced and the strain is larger for thin t_s. Additionally, shape differences and reduced surface mobilities of Ge atoms at lower T_g might influence the interaction range of strain fields originating from buried self-assembled islands.

A quantitative transmission electron microscopy (TEM) study on the degree of vertical island alignment P for fivefold 6.5-ML Ge/Si island stacks grown at $T_g=620$ °C under identical growth conditions is presented in Fig. 2(b) after Kienzle *et al.*[1] The graph reveals how the Ge island position alignment decreases with increasing Si spacer thickness. Perfect alignment is evident for $t_s\leqslant25$ nm and random island distribution is found for $t_s\geqslant100$ nm. In between a gradual transition from $P=1$ to $P=0$ is observed. From this analysis the correlation length t_{ct} is usually determined as the thick-

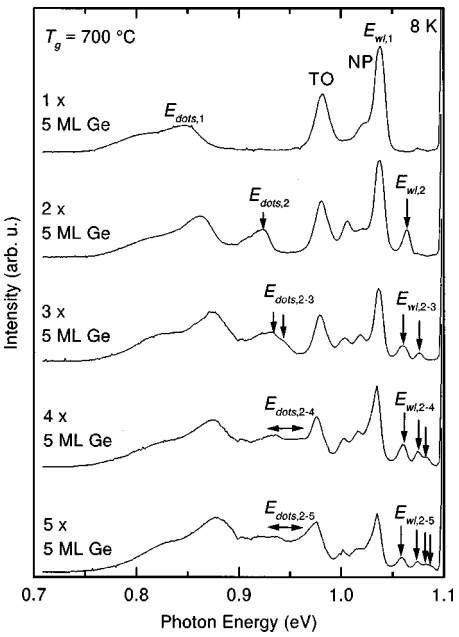

FIG. 3. Series of PL spectra where the number of island layers was changed from $n=1$ to $n=5$. The blueshifted NP lines of the nth layer are denoted by $E_{\mathrm{wl},n}$ and $E_{\mathrm{dots},n}$ for the WL and the islands, respectively. The thickness of the Si spacer layer is $t_s = 15$ nm.

ness t_s, at which P has dropped to $\frac{1}{2}$.[1,2] Hence, for our specific growth conditions $t_{ct}=70$ nm. This is in reasonable agreement with $t_{ct}=50$ nm deduced from the PL experiments, considering the relatively large error bars in Fig. 2(b) and an uncertainty in the slope of the straight line in Fig. 2(a).

We now want to use the basic ideas gained in this section to understand the PL and growth behavior in multiple island layers, where t_s is thin enough to cause vertical island alignment. We will also try to present an explanation for the blueshift of $E_{\mathrm{dots},2}$.

IV. MULTIPLE ISLAND LAYERS

Figure 3 shows the PL spectra of a series of samples where the only parameter changed was the number n of island layers deposited, ranging from $n=1$ to 5 layers. t_s was kept constant at 15 nm. Basically, we see a repetition of the effects observed for the twofold case in Fig. 1: For the nth Ge layer deposited, a blueshifted NP line of the nth WL appears at the energy $E_{\mathrm{wl},n}$. As we proposed, in Sec. IV the reduction of t_{wl} is a function of the strain-field modulation at the Si surface. In multiple island layers the strain fields from *all* buried island layers are expected to superimpose at the Si surface. This means that with increasing number of buried island layers the surface strain gradient increases and hence the critical thickness and thus t_{wl} reduces, which eventually leads to the blueshifted energy transitions (see also discussion of Fig. 4).

A repetitive behavior is also oberved for the island related PL peaks in Fig. 3, denoted by $E_{\mathrm{dots},n}$. The exact energy position of $E_{\mathrm{dots},n}$ cannot be determined for higher indexed layers, though, since PL peaks are too broad to be resolved. The general trend of a blueshift in energies is nevertheless

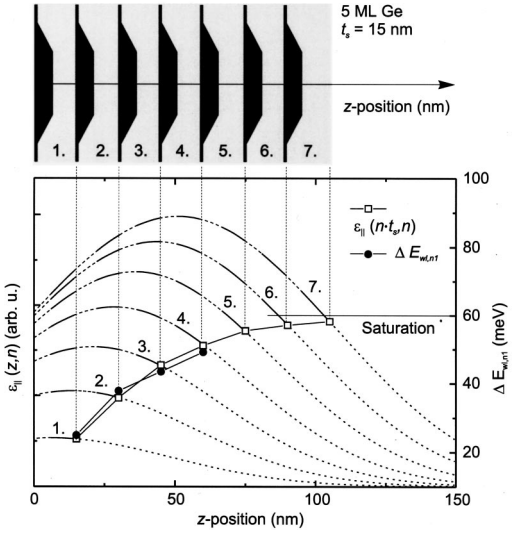

FIG. 4. In-plane strain $\epsilon_\parallel(z,n)$ along the z direction through the middle of an island stack for $n=1$ to $n=7$ island layers. $\epsilon_\parallel(z,n)$ is negative in sections where the Ge island sits. However, for clarity we interpolated those sections with dashed lines. The strain on the Si surface after growth of the Si spacer layers $\epsilon_\parallel(nt_s,n)$ is represented by open squares. Solid squares denote the PL line splitting $\Delta E_{\mathrm{wl},n1}$. Both quantities $\epsilon_\parallel(nt_s,n)$ and $\Delta E_{\mathrm{wl},n1}$ exhibit saturation.

evident and saturation with increasing n can be observed. According to Eq. (1) we define the energy separation of the nth layer as

$$\Delta E_{\mathrm{wl},n1}=E_{\mathrm{wl},n}-E_{\mathrm{wl},1}.$$

We now investigate how $\epsilon_\parallel$ changes during growth of multiple island layers. In this case $\epsilon_\parallel$ is not only a function of the z position but it also depends on the number n of deposited Ge layers. First we consider the case where island layers are capped by infinitely thick Si layers. If we assume that t_s is kept constant between layer number i and $i+1$ the strain is simply given by the sum

$$\epsilon_\parallel(z,n)=\sum_{i=1}^{n}\epsilon_\parallel(z-it_s),\quad -\infty<z<\infty, \tag{4}$$

where $\epsilon_\parallel(z-it_s)$ is given by Eq. (3), which is fitted by Eq. (2). The origin of our coordinates is always taken as the center of the initial island base. $\epsilon_\parallel(z,n)$ is shown in Fig. 4 for $n=1$ to $n=7$. As expected the maximum strain increases with increasing n and the maximum of the strain occurs at the center of the island stack, if we assume a symmetric strain-field distribution.

We are now interested in the strain state of the Si surface just before growing the next island layer, i.e., after growth of the spacer layers. In other words, we want to determine $\epsilon_\parallel(z,n)$ as defined in Eq. (4) at z positions $n\,t_s$ along the line through the center of the islands. The tensile strain $\epsilon_\parallel(nt_s,n)$ is given in Fig. 4 as open square symbols for $n=1$ to $n=7$. After the first spacer layer is grown, the Si surface is distorted by the strain field of the initial island layer. After the second spacer layer, however, the strain fields of the two buried island layers superimpose and the net strain after growth of the second spacer layer has increased. The increase is not linear in n since the strain originating from the

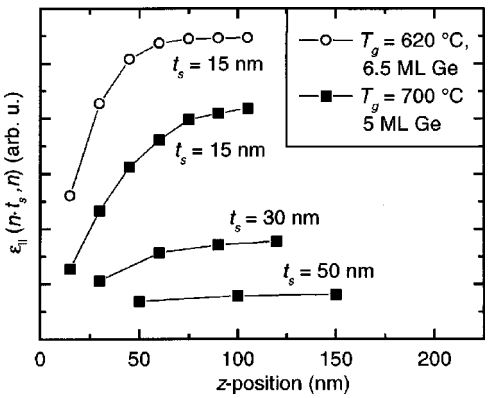

FIG. 5. $\epsilon_{\|}(nt_s,n)$ for different t_s and different growth conditions, i.e., different strain functions $\epsilon_{\|}(z)$ as determined from Fig. 2.

initial layer has already dropped by a certain amount. With increasing number of spacer layers $\epsilon_{\|}$ approaches a saturation value because the strain contribution from the nth Ge island layer is exactly compensated by the decrease of strain originating from the $n-1$ underlying island layers. Solid circles in Fig. 4 correspond to $\Delta E_{\mathrm{wl},n1}$ for $n=1$ to $n=4$ determined from our PL measurements. We see that the saturation behavior of $\Delta E_{\mathrm{wl},nl}$ is very well described by our model of strain superposition at the Si growth front.

The saturation behavior of the strain can be very different, depending on the thickness of the spacer layer and on the growth conditions selected. Figure 5 shows the strain $\epsilon_{\|}(nt_s,n)$ at the Si surface with increasing number of layers n for different t_s. Whereas for $t_s=15$ nm 90% of the saturation value is reached after five layers, for $t_s=30$ nm, saturation is already evident after two layers. The reason for this is that with increasing t_s the strain fields of underlying islands have a longer distance to attenuate. We also inserted the calculated curve for the case of 6.5-ML Ge grown at $T_g=620\,^{\circ}\mathrm{C}$ where t_s was chosen as 15 nm and $\epsilon_{\|}(z)$ was taken from Fig. 2. Since the strain-field interaction length t_{ct} is smaller than for $T_g=700\,^{\circ}\mathrm{C}$ saturation sets in much earlier.

V. MATERIAL INTERDIFFUSION

We now present a model that possibly explains the blueshifted PL originating from the stacked Ge islands in Figs. 1 and 3. For this purpose we qualitatively consider the strain and strain energy at the Si surface above a buried Ge island. Such a situation is illustrated in Fig. 6(a). A single layer of Ge islands has been grown and is covered with a thin Si cap layer. In this case we assume that there has been no SiGe material interdiffusion during overgrowth. Since the Ge island has partially relaxed elastically, we find a strain modulation on the Si surface. Above the island the Si matrix is laterally widened and the surface exhibits tensile strain. Since we only consider pseudomorphic layers the tensile strain must be accommodated in neighboring regions as compressive strain and $\epsilon_{\|}$ becomes negative. Hence, the surface exhibits a strain modulation and $\epsilon_{\|}(x)$ as a function of the lateral position x is schematically given in the middle part of Fig. 6(a). A very similar strain modulation for InAs/GaAs quantum dots was found in Ref. 17. At the top we also show $\epsilon_{\|}^2(x)$, which is proportional to the tensile strain energy. In Fig. 6(b) we consider an island that has intermixed with Si during overgrowth. As a result the tensile strain at the Si surface above the SiGe island exhibits reduced strain modulation, leading directly to lower strain energy at the surface. From an energetic point of view the case of SiGe intermixing is more favorable than no intermixing. In fact, the total strain energy for the whole system would be minimized by a transformation of the Ge island into an alloyed SiGe quantum well[18] but kinetic limitations during overgrowth naturally prevent this idealized case. The tendency for SiGe intermixing is also well reflected in PL spectra where simple estimations of confinement and band-edge alignments in embedded Ge/Si islands yield a SiGe interdiffusion of 40–60 %.[19]

The arrangement of stacked islands is presented in Fig. 6(c). As we know from Fig. 6(b) the island in the first layer has intermixed with Si. However, the island still experiences some strain field in the z direction and the island in the second layer sits exactly on top of the first island. Since $t_s < t_{ct}$ the second WL is thinner than the initial one and the Ge island will be slightly larger than that in Fig. 6(a). In order to compare to Fig. 6(a) we again assume that the second island has not intermixed during overgrowth. As we have shown in Figs. 4 and 5 the net strain at the Si surface of covered stacked islands is larger than for a single island layer since strain fields of underlying islands add up. Hence, not only the strain field but also the strain energy modulation at the Si surface of the twofold stack is enhanced compared to the case of only one island. As a consequence strain gradients and the effect of SiGe intermixing are more pronounced in stacked layers in order to release strain energy as is schematically illustrated in Fig. 6(d). The enhanced material intermixing in stacked island layers cause the PL blueshift with increasing number of island layers (Fig. 3), and and with reduced t_s (Fig. 1). The degree of intermixing is likely to saturate with increasing number of layers, as the strain fields also saturate. In fact, in Fig. 3 there is not a lot of difference between the island related PL of the fourfold and fivefold stack. Although we discussed the case of completely capped Ge islands, very similar arguments apply during the Si overgrowth process itself, where the actual alloying process takes place.

In Ref. 9 we suggested that strain relaxation within the islands would cause a blueshift in PL energy. Strain fields are of long range and usually the interaction range in the z direction is much larger than the height of the islands. If we consider the strain distribution $\epsilon_{\|}(z,n=2)$ in Fig. 4 we see that the maximum strain occurs in the middle of the two islands and the curve is almost symmetric in the z direction. Asymmetry due to island shape and WL positions are negligible in this island configuration.[9] Hence, the effect of strain in embedded islands should change the band-edge alignment in the twofold island layers in a symmetric way and cause either a redshift or blueshift in both $E_{\mathrm{dots},1}$ and $E_{\mathrm{dots},2}$. Also, for small t_s in the case of carrier tunneling, where the transition associated with the initial island layer is the main peak seen in PL, no substantantial blueshift is observed for $E_{\mathrm{dots},1}$. This is why we think that the main contribution for the PL blueshift originates from the material interdiffusion during overgrowth and not from strain induced band-edge modifications. However, we cannot rule out certain asymetric

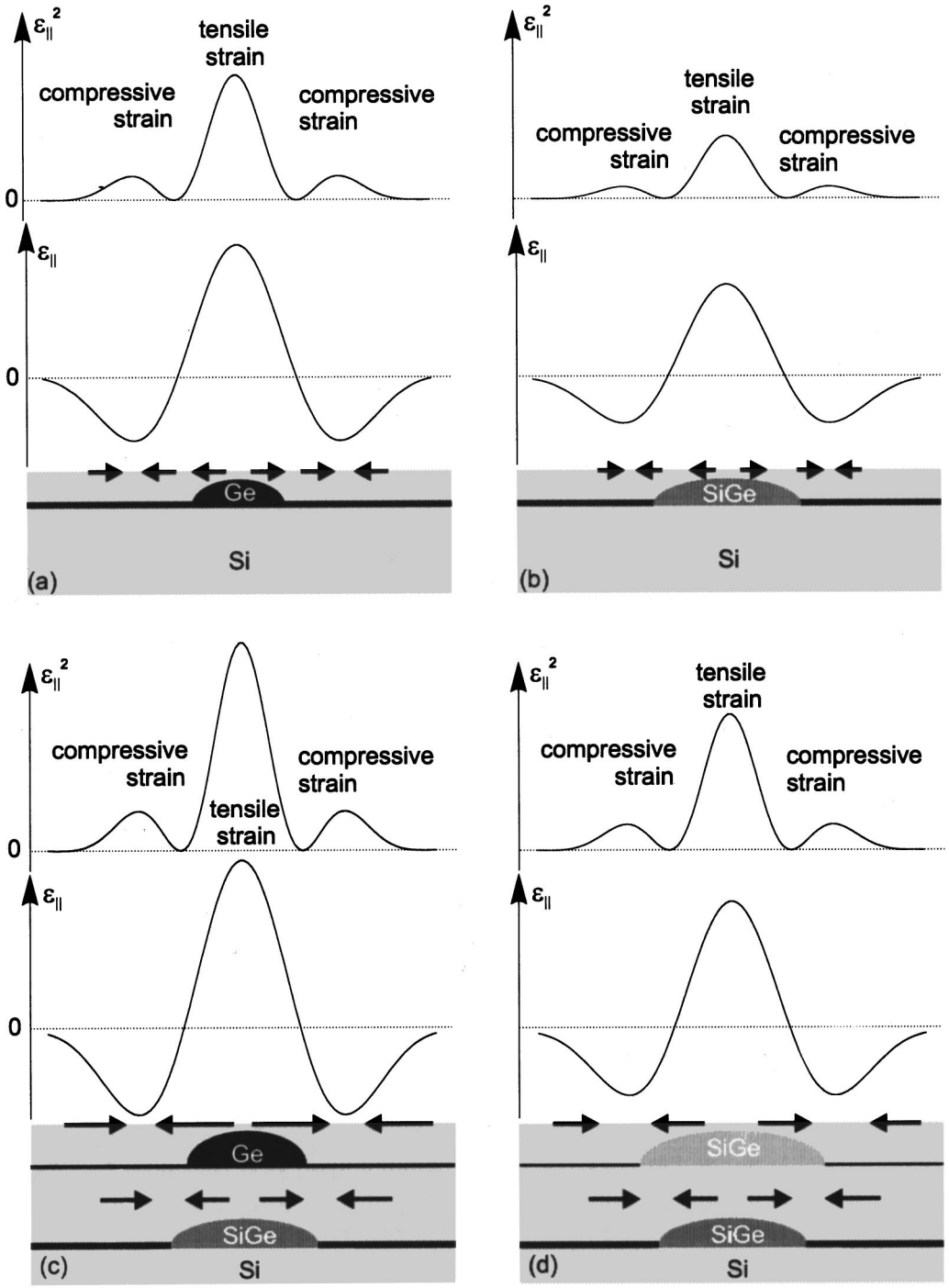

FIG. 6. Schematic illustration of the in-plane strain and tensile strain energy modulation at the Si surface after the Ge island has been just been covered with Si. (a) shows the case of a single, nonintermixed Ge island, (b) illustrates the situation for a SiGe island, in (c) the combination of vertically aligned Ge islands is shown, where the initial island has intermixed and the second has not. In (d) intermixing is most pronounced since in (c) strain energy is largest.

charge carrier dynamics in and around the islands, and a much more detailed study would be needed to fully understand the recombination processes in stacked Ge/Si islands.

To present further evidence for our model, Fig. 7 shows a cross-section bright-field TEM image of a fivefold 6.5-ML Ge island stack grown at $T_g = 620\,^{\circ}\mathrm{C}$, where t_s was kept constant at 13 nm. On top of a 100-nm-thick Si cap layer a single 6.5-ML Ge island layer was deposited. The difference between the uncapped and the capped Ge islands is very striking. Whereas the diameter to height ratio R of the uncapped island is about 6 (also compare AFM data from Fig. 10) the capped island in the initial layer exhibits a ratio of about 14.5. This difference reflects the strain considerations and the SiGe intermixing effects we discussed in Fig. 6, i.e., due to strain energy minimizations the capped island is driven to a much flatter structure towards the energetically favorable quantum well case. In addition, we can see that with increasing number of Ge layers the islands become larger in the lateral direction whereas the height stays more or less constant. In Fig. 7 we plot R as a function of layer

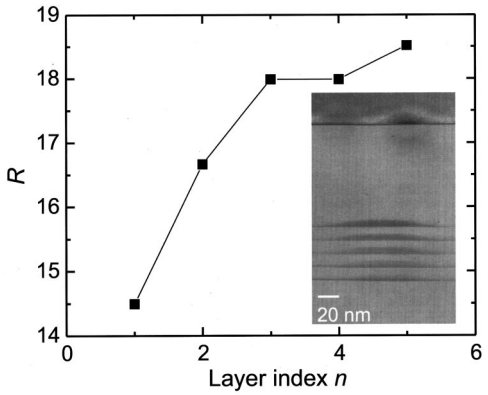

FIG. 7. Diameter to height ratio R of islands in stacked layers. The data is deduced from the cross-section TEM image shown as an inset.

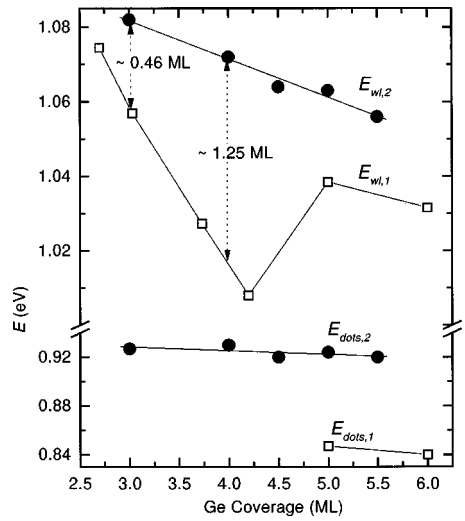

FIG. 8. Wetting layer related and island related NP energies for two series of samples. The open squares are taken from samples incorporating only a single embedded Ge layer and the energies are denoted by $E_{\mathrm{wl},s}$ and $E_{\mathrm{dots},s}$ for the WL and the islands, respectively. $E_{\mathrm{wl},2}$ and $E_{\mathrm{dots},2}$ denote the island and WL NP energies originating from the second Ge island layer in a twofold Ge island stack. In this series the Ge coverage for the initial Ge layer was kept constant at 5 ML and the spacer thickness was 15 nm.

index n. There is an initial increase in R with increasing n, followed by a saturation for larger n, and eventually R reaches an equlibrium value. This result supports the model of strain-field-dependent SiGe alloying in stacked islands layers, which saturates for larger n. As a matter of fact, recently Mateeva *et al.*[3] reported TEM investigations on 20-fold Ge/Si island stacks. In that work they saw a shape transformation of islands in the initial layers and a stabilization of island size and shape in layers with higher index. Apart from lateral merging of islands we think that the saturation effect of surface strain with increasing number of grown island layers eventually causes equilibrium island shapes and sizes within the hole stack.

Finally, we want to note that it is mainly the large size of self-assembled Ge islands that allows one to separate confinement effects, material intermixing, and strain effects in PL experiments. If islands are so small that the lateral extension also contributes to carrier confinement (like in the case of many III/V material-based quantum dot heterostructures) this separation is much more difficult to perform since many different effects participate and shift the island related energy transitions. Hence, the Ge/Si material system is well suited as a model system to investigate and understand fundamental effects on the optical and electronic properties of self-assembled island and quantum dot heterostructures and might be helpful to other semiconductor material combinations.

VI. ASYMMETRIC Ge DEPOSITION IN TWOFOLD STACKS OF ISLANDS

In the following we investigate the case of asymmetric Ge deposition in twofold Ge island stacks, i.e., we deposit less Ge in the second island layer. Figure 8 shows the energy position of the wetting layer and the islands for two series of samples. In a first reference series only a single sheet of islands with varying Ge deposition was embedded in Si (open squares), and the corresponding energy of the PL transitions are marked by $E_{\mathrm{wl},1}$ for the wetting layer and $E_{\mathrm{dots},1}$ for the islands. In the second series, twofold stacked island layers were grown, where the Ge coverage in the initial layer was kept constant at 5 ML and the Ge deposition in the second layer was varied from 3 to 5 ML (full dots). t_s was 15 nm in all samples. The PL energies for the wetting layer and islands in the second layer are marked $E_{\mathrm{wl},2}$ and $E_{\mathrm{dots},2}$, respectively.

$E_{\mathrm{wl},1}$ and $E_{\mathrm{dots},1}$ show the usual behavior as observed for single sheets of Ge islands.[7,8] Up to the critical thickness t_c of about 4.5 ML, only PL from the wetting layer is observed. Once t_c is passed a broad PL peak $E_{\mathrm{dots},1}$ originating from the islands appears at lower energies. Note, that in the course of island formation $E_{\mathrm{wl},1}$ is blueshifted by about 26 meV, which is attributed to Oswald ripening of the islands.[7,8] For the twofold stacks, island formation is already evident for Ge coverage as low as 3 ML in the second layer. This is reflected by the blueshifted $E_{\mathrm{wl},2}$ at 1.082 eV and an island related transition at 0.927 eV, which is slightly less intense than the PL peak from the initial island layer. The shift of $E_{\mathrm{dots},2}$ to high energies as compared to $E_{\mathrm{dots},1}$ is explained by enhanced intermixing in the second layer as discussed in Sec. V.

With increasing Ge coverage $E_{\mathrm{wl},2}$ slightly shifts to lower energies. This redshift has a different physical origin than that of $E_{\mathrm{wl},1}$ for Ge depositions less than 4.2 ML. For $E_{\mathrm{wl},1}$ the redshift is caused by a decrease of the confinement energy along the growth direction with increasing t_{wl} below the critical thickness for island nucleation, whereas the decrease of $E_{\mathrm{wl},2}$ is attributed to a slight increase of t_{wl} after the onset of the island formation (similar to the decrease of $E_{\mathrm{wl},1}$ for Ge coverages larger than 5 ML).

From the difference $E_{\mathrm{wl},2}-E_{\mathrm{wl},1}$ we derive that 0.46 ML excess Ge material from the wetting layer is available to form the islands in the second layer. With increasing Ge coverage this excess material gradually increases, e.g., at 4 ML it is already about 1.25 ML Ge.[20] Surprisingly, $E_{\mathrm{dots},2}$ stays almost unaffected by the material increase at about 0.92 eV.

Figure 9 shows $2\times 2\ \mu\mathrm{m}^2$ AFM scans of the surface morphology for different Ge coverages in the second island

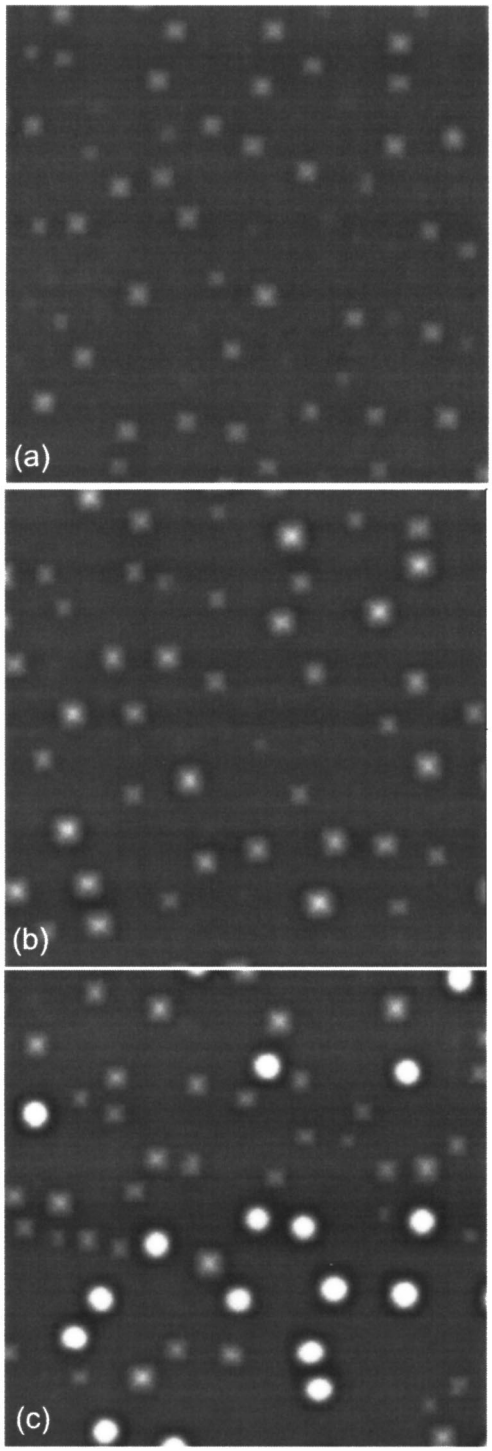

FIG. 9. ($2\times2\ \mu m^2$) AFM scans of (a) 3-ML Ge, (b) 4-ML, and (c) 5-ML Ge. Each Ge layer was deposited on top of an initial 5-ML-thick Ge island layer capped by 15-nm-thick Si. Note that even for 3-ML Ge well-developed islands are visible.

layer. Figures 9(a) and 9(b) correspond to 3 and 4 ML Ge, respectively—Ge coverages at which no islands would have formed without the first Ge island layer. The images only reveal pyramidal shaped islands. In Fig. 9(c), 5 ML Ge was deposited and two distinct types of islands are evident: large domes and much flatter pyramids, as is typical in Ge/Si growth for certain growth conditions.[9,11–13] The areal island density stays about the same for all Ge depositions at 1.5

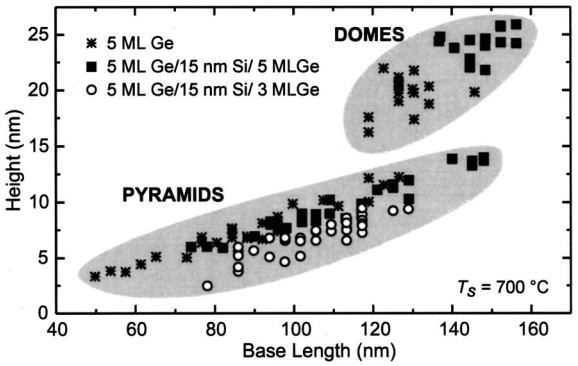

FIG. 10. Island height as a function of diameter for a single layer of 5-ML Ge, two stacked 5-ML layers, and 3-ML Ge grown on top of an initial 5-ML Ge layer.

$\times10^9\ cm^{-2}$, as would be expected for $t_s=15$ nm, where we have 100% vertical alignment. An improvement of the island size inhomogeneity is not observed.

The three AFM images nicely illustrate that pyramids constitute a metastable island phase, which directly transform into multifaceted domes with increasing Ge deposition.[21,22] It should be noted that often Si-rich SiGe layers have been grown on Si at high T_g to study this effect, since the reduced lattice mismatch allows for a more gradual island transformation from pyramids to domes.[22] The same effect applies to our case, where the effective lattice mismatch between islands and Si spacer layer is reduced by the strain fields of buried islands. Hence, the arrangement of stacked islands offers the opportunity to select pure Ge pyramids in a very controllable way.

An even better understanding of the island formation can be obtained if we plot the height of the islands as a function of their diameter. In Fig. 10 the height-base length data are depicted for a single 5 ML thick Ge sample and the two samples shown in Figs. 9(a) and 9(c), respectively. The two different island phases exhibit different height to diameter ratios and are therefore well separated in this graph. Like the stacked 5 ML Ge/15 nm Si/5 ML Ge sample the single Ge layer also exhibits two types of islands. Hence, it is possible that the two shoulders of the island related PL, which we observed in Fig. 1, originate from the NP transition of domes and pyramids and are not the NP and TO phonon replica of a single type of islands.[23] Note, that phononless radiative recombination of Ge islands was demonstrated in Ref. 26. Likewise, the two blueshifted lines in the twofold stack in Fig. 1 might originate from the two different island shapes although the energy difference between the two peaks is about 59 meV, which is very similar to the Si-Si TO phonon energy. In addition we also note that pyramid heights in the stacked 5 ML Ge/15 nm Si/3 ML sample are only slightly smaller than those in the stacked 5 ML Ge/15-nm Si/5 ML sample. This would explain why $E_{dots,2}$ stays relatively constant in energy with increasing Ge coverage in Fig. 8.

Compared to the single layer, the twofold 5 ML Ge stack exhibits on average larger domes and pyramids, which is a direct consequence of the reduced t_{wl} in the second layer. The size increase is *not* due to the coalescence of islands since the island density is the same for both the single and the twofold layers. We observe a slightly different height to

base length ratio for the 5 ML Ge/15 nm Si/3 ML Ge sample and AFM linescans across the center of the islands reveal that most of the pyramids are truncated. Unlike single layers, islands on top of an initial seeding layer seem to start nucleation with very flat and truncated pyramids, which become fully developed in the later stage of nucleation (see 5 ML/15-nm Si/5-ML sample). We attribute this difference in island formation to the strain field modification below the islands.

VII. CONCLUSIONS

We have presented a systematic PL study on twofold stacks of Ge islands where an energy separation between the WL related energy transitions ΔE_{wl} is observed. ΔE_{wl} is caused by a reduction of the critical thickness in the second layer and was shown to probe the strain fields created by buried island layers. Based on our experimental results we have evaluated the in-plane strain at the Si surface with increasing number of deposited island layers. Our calculations qualitatively explain enhanced SiGe intermixing in stacked islands that results in the observed blueshift of the island related PL transitions. Recently observed shape transformations for buried Ge islands are well explained by our model of superimposed strain fields. We also report PL and AFM data on the initial stages of island formation in the second layer of twofold island stacks, where the transformation from pyramids to domes is well documented. Our PL results on multiple island sheets imply that resonant emission from stacked islands is spoiled by material intermixing effects, and a careful tuning of the overgrowth temperature might be necessary to tackle this problem. Our results can be helpful to other self-assembled island and quantum dot heterostructures where separation of confinement, strain, and size effects is more difficult due to smaller dot sizes.

ACKNOWLEDGMENTS

We thank Y. Rau for the finite element calculation and O. Kienzle and F. Ernst for one cross-section TEM image.

[1] O. Kienzle, F. Ernst, M. Rühle, O. G. Schmidt, and K. Eberl, Appl. Phys. Lett. **74**, 269 (1999).
[2] B. Rahmati, W. Jäger, H. Trinkaus, R. Loo, L. Vescan, and H. Lüth, Appl. Phys. A: Mater. Sci. Process. **62**, 575 (1996).
[3] E. Mateeva, P. Sutter, J. C. Bean, and M. G. Lagally, Appl. Phys. Lett. **71**, 3233 (1997).
[4] G. Abstreiter, P. Schittenhelm, C. Engel, E. Silveira, A. Zrenner, D. Mertens, and W. Jäger, Semicond. Sci. Technol. **11**, 1521 (1996).
[5] J. Tersoff, C. Teichert, and M. G. Lagally, Phys. Rev. Lett. **76**, 1675 (1996).
[6] C. Teichert, M. G. Lagally, L. J. Peticolas, J. C. Bean, and J. Tersoff, Phys. Rev. B **53**, 16 334 (1996).
[7] H. Sunamura, N. Usami, Y. Shiraki, and S. Fukatsu, Appl. Phys. Lett. **66**, 3024 (1995).
[8] O. G. Schmidt, C. Lange, and K. Eberl, Appl. Phys. Lett. **75**, 1905 (1999).
[9] O. G. Schmidt, O. Kienzle, Y. Hao, K. Eberl, and F. Ernst, Appl. Phys. Lett. **74**, 1272 (1999).
[10] M. Goryll, L. Vescan, and H. Lüth, Thin Solid Films **336**, 244 (1998).
[11] G. Medeiros-Ribeiro, A. M. Bratkovski, T. I. Kamins, D. A. A. Ohlberg, and R. S. Williams, Science **279**, 353 (1998).
[12] M. Goryll, L. Vescan, K. Schmidt, S. Mesters, H. Lüth, and K. Szot, Appl. Phys. Lett. **71**, 410 (1997).
[13] T. I. Kamins, G. Medeiros-Ribeiro, D. A. A. Ohlberg, and R. S. Williams, J. Appl. Phys. **85**, 1159 (1999), and references therein.
[14] S. Christiansen, M. Albrecht, and H. P. Strunk, Appl. Phys. Lett. **64**, 3617 (1994).
[15] Q. Xie, A. Madhukar, P. Chen, and N. P. Kobayashi, Phys. Rev. Lett. **75**, 2542 (1995).
[16] G. Wöhl, C. Schöllhorn, O. G. Schmidt, K. Brunner, K. Eberl, and O. Kienzle, Thin Solid Films **321**, 86 (1998).
[17] M. Grundmann, R. Heitz, N. Ledentsov, O. Stier, D. Bimberg, V. M. Ustinov, P. S. Kop'ev, Zh. I. Alferov, S. S. Ruvimov, P. Werner, U. Gösele, and J. Heydenreich, Superlattices Microstruct. **19**, 81 (1996).
[18] S. Christiansen (private communication).
[19] O. G. Schmidt (unpublished).
[20] Note that the values for excess material present only a lower limit, since Ge segregation effects would increase the amount of Ge material that is available in the second island layer.
[21] T. I. Kamins, E. C. Carr, R. S. Williams, and S. J. Rosner, J. Appl. Phys. **81**, 211 (1997).
[22] J. A. Floro, G. A. Locadomo, E. Chason, L. B. Freund, M. Sinclair, R. D. Twesten, and R. Q. Hwang, Phys. Rev. Lett. **80**, 4717 (1998).
[23] A quantitative evaluation of confinement energies in buried domes and pyramids is not possible to give at the present stage of research. This is due to the fact that energy transitions will not only depend on the height of buried islands but also on the strain state of the islands and on the degree of material mixing, which again depends on the exact strain state of the free standing island. Additionally, the in-plane tensile strain in the Si between two vertically aligned islands is likely to create localization potentials for electrons (Refs. 24 and 25) and the depth of these potentials are again dependent on the strain state of the islands.
[24] O. G. Schmidt, Ph.D. thesis, Max-Planck-Institut für Festkörperforschung, Stuttgart, Germany, 1999.
[25] K. Eberl, O. G. Schmidt, O. Kienzle, and F. Ernst, Solid State Phenom. **69-70**, 13 (1999).
[26] S. Fukatsu, H. Sunamura, Y. Shiraki, and S. Komiyama, Appl. Phys. Lett. **71**, 258 (1997).